



Operated for NASA by AURA

Instrument Science Report TEL 2009-01

# FGS2r: Deadtime, Background, Photon Aging, Sensitivity Calibrations, and Noise Properties

---

R. L. Gilliland, R. C. Bohlin, P. R. McCullough, & E. Nelan

gillil@stsci.edu

April 2009

---

## Abstract

Execution of a large science program using FGS2r on a very bright target for which accurate knowledge of deadtime corrections was needed has led to this and closely related calibrations. FGS2r had not previously been used for science; and, thus, accurate calibrations had not been needed in the past. Using calibration observations obtained in support of the large science program we will derive accurate values for the deadtime corrections for each of the four PMTs that support relative correction accuracies of -0.7% to +0.6% at the count level of the science target motivating this study. Typical background levels resulting from detector noise and sky are a necessary input for the deadtime calibration. A determination of sensitivity (count rate as function of  $V$ ) is readily available and quoted. The large science program counted some  $1.0 \times 10^{12}$  photons over 10 days; those observations, and separate before and after observations of the FGS standard Upgren 69 quantify the small resulting sensitivity loss.

Deadtime corrections across the 4 PMTs in FGS2r differ by nearly 50%, suggesting that the single canonical value usually assumed does not suffice for accurate work at high count rates on any of the FGSs without similar on-orbit calibrations.

---

## 1. Introduction

FGS science observations became very common in the fall of 2008 with both general science instrument (STIS, ACS, NICMOS) failures having accrued over the years, and a

fortunately temporary period between loss of the HST Side A SI-C&DH, and resumption of Side B operations when the FGS was the only usable science instrument. One FGS science program in particular imposed unique stresses and requirements. GO/DD-11945, Asteroseismology of Extrasolar Planet Host Stars, was approved to observe a  $V = 8.17$  target (HD 17156) for a nearly continuous 10-day period over 2008 December 22-31 during which time some  $10^{12}$  photons would be counted as required to detect oscillations at amplitudes of only a few parts per million. Engineers were concerned initially that such a high photon flux, over such a long time, which was far beyond anything previously attempted could pose a hazard for the FGSs through PMT aging and lost sensitivity. Although further investigation suggested likelihood of such lost sensitivity being significant (e.g. several per cent) was negligible; nonetheless, this large science program was required to use FGS2r, which is expected to have a limited lifetime from other causes and is scheduled for replacement in the next servicing mission. Thus, FGS2r was used for a 175 orbit science program, its first such use.

One component of the GO/DD-11945 program is to measure very accurately the light curve resulting from transits of the planet HD 17156b across its host star. From ground based photometry this transit depth is known to be about 0.5%. The relative area of the planet to that of the star scales as this transit depth. At the count rates expected for HD 17156, about  $4 \times 10^5$  counts per second per PMT and with a nominal deadtime of 285 nanosecs (Nelan et al. 2007), the implied adjustment of 11.4% for deadtime directly translates into an expansion of the FGS-observed transit depth by this amount. For the science, the transit must be measured as accurately as possible; Poisson statistics alone would support per-transit (three were obtained) depth determinations to  $\sim 20$  ppm (parts per million). Fractionally, the latter is 0.004, or 0.4% of the 0.5% transit depth. To avoid larger systematics from the deadtime correction, the deadtime correction constant for each PMT separately must be determined sufficiently well to support this.

The detector deadtime results from the PMT and associated pulse sampling electronics being unable to sense a newly arrived photon within the deadtime,  $T_D$ , after a previously detected photon. The mean time to detect a photon is  $T_D + 1/C_T$ , where  $C_T$  is the true photon arrival rate. This results in a detection rate of:

$$C_M = C_T / (1.0 + T_D C_T) \tag{1}$$

where  $C_M$  is the measured count rate. This implicit equation for the desired true rate may be rewritten as:

$$C_T = C_M / (1.0 - T_D C_M) \tag{2}$$

For the FGSs which have a natural sampling interval of 0.025 seconds (40 Hz), the deadtime

correction equation is usually written as:

$$C_T = C_M / (1.0 - C_M(T_D/T_I)) \quad (3)$$

where the  $C$ 's are now the number of counts within the sampling interval of  $T_I = 0.025$  seconds rather than per second rates, a convention we will now adopt. Eq. (3) and associated discussion were presented in Lattanzi and Taff (1993), the only FGS ISR related to deadtime calibrations. Lattanzi and Taff refer to a pre-flight determination of 285 nanoseconds for the deadtime coefficient,  $T_D$  and note that no on-orbit calibrations were anticipated. Lattanzi and Taff also quote an implied correction for the  $V = 9.6$  standard star Upgren 69 of 0.09 mag, while our new calibration determines this to be 0.03 mag (the simplest explanation would be that the previous study inappropriately used the sum over all 4 PMTs as the measured value to correct, while the correction is defined to be on a per PMT basis).

Assuming that this simple equation holds over the necessary intensity interval, obtaining a calibration of  $T_D$  can be reduced to measuring the relative count rates in two stars of accurately known relative brightness. The FGS bandpass and sensitivity as a function of wavelength is not well quantified, therefore it is important for the two calibration stars to have similar spectral energy distributions. The two stars should provide excellent leverage, ideally with one star somewhat brighter than HD 17156, and the other significantly fainter. The faint star should still be bright enough that normal sky background uncertainties do not become a significant error budget term. We chose two STIS spectrophotometric standards, HD 209458 at  $V = 7.65$ , and P041C at  $V = 12.00$ , both of which are close to solar spectral types. In principle this calibration is straightforward, in practice given non-identical spectral energy distributions for the stars, considerable attention is required to constrain the FGS sensitivity with wavelength for each PMT in FGS2r. Similarly, at our required accuracy level, there are several liens that need to be retired; and cross-checks must be made to establish a trusted calibration.

A complication for photon counting systems suffering from deadtime effects is that the electronics may provide two distinct ranges of behavior. In a “Nonparalyzable” system the counting is disabled for the time  $T_D$  after a recorded event, but then regains sensitivity. Equations (1)-(3) above are precise (even for the stringent needs of GO/DD-11945) representations for nonparalyzable detectors (Evans 1955). In a “Paralyzable” system the next output count cannot occur until there is a time interval of at least  $T_D$  between two successive true count inputs, and the observed and true counts are related as (Evans 1955):

$$C_M = C_T \exp(-C_T(T_D/T_I)). \quad (4)$$

See also Zhang et al (1995) for independent presentations and discussions of the same equations. Detector systems can show intermediate behavior, or as in our cautionary

Table 1: FGS2r Dark Counts

PMT	Counts at 40 Hz	Error
$A_X$	3.880	0.17
$B_X$	2.715	0.10
$A_Y$	2.592	0.01
$B_Y$	2.034	0.04

discussion in §3.4 other more complicated responses not captured by Eqs. (3) or (4). At the risk of confusing an unwary reader we will carry independent results for Eqs (3) and (4), resulting in significantly different deadtime coefficients, although the difference in Eqs (3) and (4) in terms of  $C_M/C_T$  values vary by less than 0.5% over the full range of rates relevant to the FGSs and these calibrations.

Because the dark current calibration is required as input to the deadtime calibration, we address determination of dark current first. Details of deadtime calibration will comprise the primary §3 of this ISR. In §4, the general sensitivity of FGS2r will be derived, and limits will be set on the brightest star that can be observed for science. The effects of having detected a trillion photons over ten days will be assessed in §5 with a discussion of photon aging of the photocathode responses. Finally, the noise properties of FGS data corrected for deadtime will be discussed in §6. For the reader interested only in bottomline results for a deadtime correction to use, we recommend selecting Eq. (3), and the “Case 2” line from Table 3 giving the deadtime constants by PMT for Eq. (3).

## 2. Dark Current

Dark current measurements have been made previously for past science FGSs by observing blank regions of sky in TRANs mode. As part of GO/DD-11945 one orbit observing a blank sky region was executed just before, and one shortly after the 10-day run on HD 17156. The two visits were numbered 70 and 82. For each of these the data were extracted to standard 40 Hz format giving the number of counts in each PMT per 0.025 second. The first 4500 lines in each data set were skipped, thus placing data use after the standard TRANs mode scanning had started. A 40-minute interval for each was then plotted and carefully inspected to be assured that no significant changes in count rate, e.g. as might happen if a faint star were crossed, the bright Earth limb approached closely, or the SAA skirted. Seeing no such perturbations in either of the visits, a grand average in terms of counts per PMT is derived and presented in Table 1.

The quoted error represents for each PMT the difference between results for visits 70 and 82. These background rates for FGS2r are within the range shown in Table 2.1 of the FGS Instrument Handbook (Nelán et al 2007) for FGS1r. With an effective aperture of  $5 \times 5$  arcsecs and nominal sky background levels of  $V \sim 22$  per square arcsec, count rates from sky are expected to be about 0.5 – 0.7 counts at 40 Hz. Thus, most of the background comes from intrinsic detector noise. Backgrounds are generally highest for the least sensitive PMTs, because such PMTs have the gain (high voltage) set at a higher level to in part compensate for the “insensitivity” of the PMT. A reasonable estimate is that backgrounds under normal circumstances (away from SAA and bright Earth limb) may vary by about 5%. The full 10-day observing sequence on HD 17156 in GO/DD-11945 always used a faint guide star in FGS3 providing useful statistics of orbit-to-orbit background variations. These showed a full range (averaged over the 4 PMTs) of only 0.2 in the units of Table 1, and an *rms* < 0.1.

### 3. Deadtime

For a calibration of the deadtime correction, new FGS2r observations were obtained of two stars of roughly solar spectral type: P041C and HD 209458.

At  $V = 12.00$ , P041C provides 250 – 350 counts at 40 Hz per PMT. At this level any deadtime corrections are minimal but will be implicitly taken into account. With the assumption of a 5% uncertainty in the sky+dark values of Table 1, these background fluctuations of 0.1 – 0.2 counts at 40 Hz induce relative uncertainties at less than the part per thousand level in the P041C counts. Averaged over 40 minutes, the Poisson statistics per PMT correspond to a maximum uncertainty level of 0.2 parts per thousand.

#### 3.1. STIS Observations of P041C and HD 209458

P041C is one of the “solar analog” calibration stars suggested by the NICMOS IDT and has been extensively observed with FOS, STIS, NICMOS, and even WFPC2.

HD 209458 was the first star with a detected transiting extrasolar planet and has been the target of extensive observations with HST. In particular, STIS observations exist in a broad 2 arcsec photometric slit for each of G430L and G750L at 4 separate epochs of 5 orbits. Typical observations provided spectra just below detector saturation at a cadence of order one minute. About 15% of the HST orbits occurred in whole or part during the HD 209458b transit with a depth of  $\sim 1.6\%$ ; orbits intersecting the transit were not used in these calibrations. HD 209458 was promoted to ‘calibration standard’ status based on the extensive existing observations from science programs GO-9055 and GO-9477. Its demonstrated constancy and NICMOS grism spectroscopy make HD 209458 the brightest source in calibrating the NICMOS count rate nonlinearity (Bohlin et al. 2006). HD209458

has a similar spectral type to P041C and is about 0.5 magnitudes brighter than HD 17156, for which the deadtime calibration is needed, but is still faint enough to not “saturate” the FGS counts at  $2^{16}$  per 40 Hz.

Over the 4200–7200 Å range of the FGS F583W filter, the STIS spectrophotometry of P041C in the wide 52X2 photometric slit is composed of the average of five G430L plus two G750L observations with a join at 5450 Å. Before converting to absolute flux, the observed count rates are corrected for the change of sensitivity with time and temperature (Stys et al. 2004) and for the CTE charge loss in the CCD detector (Goudfrooij & Bohlin 2006). This spectrophotometry is discussed in Bohlin, Dickinson, & Calzetti (2001) and in Bohlin (2007). The absolute flux distributions for both P041C and HD209458 are available from the CALSPEC database.<sup>1</sup>

Any uncertainty due to Poisson statistics is negligible over the 4400 – 7100 Å range of the half peak transmission wavelengths for the FGS F583W. For example, the total detected photoelectrons for P041C from 4400–7100 Å are  $4 \times 10^8$ . The uncertainty in the ratio of P041C to HD 209458 is dominated by uncertainties in the repeatability of STIS spectrophotometry and in the CTE correction for non-linear response. Figure 1 of Bohlin & Gilliland (2004) shows the repeatability for 47 G430L and 43 G750L observations of the bright star AGK+81°266 ( $V=11.94$ ). Over the F583W range of 4400–5450 Å that falls within the G430L mode, the average repeatability is 0.35% in 200Å bins, while the corresponding rms scatter for G750L is 0.18% in 400 Å bins over the 5450–7100 Å range. The rms  $1\sigma$  values over the 1050 and 1650 Å full range in G430L and G750L, respectively, should be lower but probably not by as much as the square root of the number of 200 or 400 Å bins. The 0.35 and 0.18% values are safe upper limits to the repeatability in the two separate modes. The weighted average over the full 4400–7100 Å F583W range is 0.25%  $1\sigma$  uncertainty from repeatability measures on the bright star AGK+81°266.

The overall signal to noise of the HD 209458 spectroscopy is extremely high using an average over four each of G430L and G750L orbit-averaged spectra obtained out of transit, and from separate visits. The repeatability in the F583W bandpass over eight separate visits is consistent with the 0.25% value for P041C discussed above.

The CTE corrections for P041C are minimal because the data were obtained in the first year of the STIS mission before the CCD detector sustained much radiation damage. The CTE corrections for HD209458 are also low, because the star is so bright. Goudfrooij & Bohlin (2006) estimate that their CTE correction algorithm is accurate to 5–10% of the amount of the correction, so that with maximum CTE corrections over the 4400–7100Å range of 0.18% for P041C and 0.14% for HD209458, the uncertainty in the CTE corrections can be neglected.

<sup>1</sup><http://www.stsci.edu/hst/observatory/cdbs/calspec.html/>.

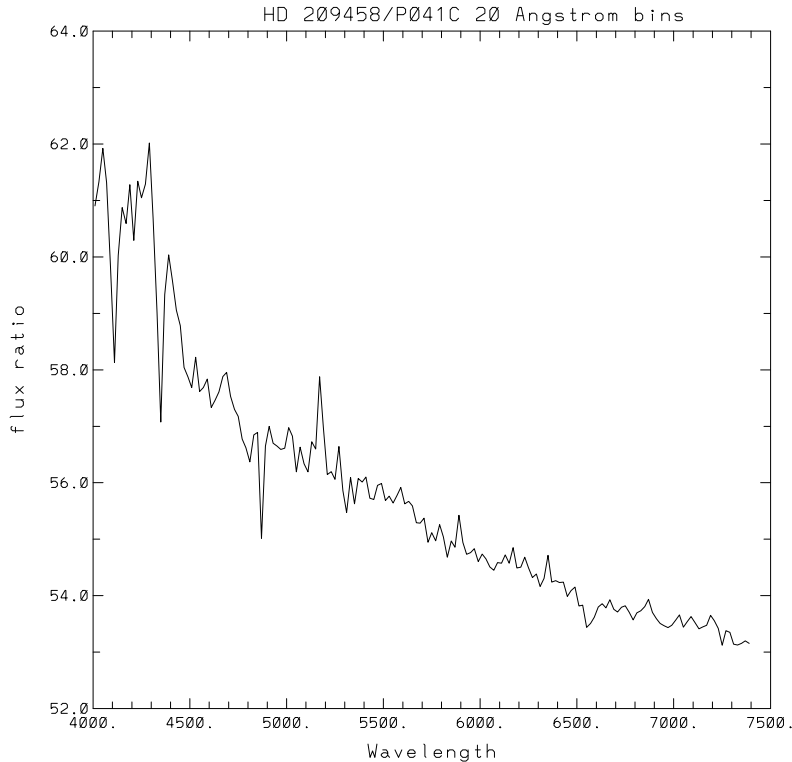


Fig. 1.— The ratio after binning to 20 Å intervals of the HD 209458 and P041C spectrophotometry. Some of the apparent noise in the ratio is due to small differences in the strength of spectral features that do not cause noise in the ratio of the separate average fluxes over the F583W bandpass.

The ratio of the merged spectra for P041C and HD 209458 are shown in Figure 1 for common 20 Å intervals. With an uncertainty of 0.25% for each star, a conservative upper limit to the precision of the ratio of P041C to HD209458 in F583W is 0.35% over the 4400–7100Å F583W bandpass. Stellar variability is expected to cause smaller uncertainties for these two stars.

One additional factor that should be considered in assessing potential deadtime calibration errors arising from P041C and HD 209458 observations is the potential for contamination from nearby sources. The STIS observations effectively integrate over 2 arcsec in dispersion (slit width on the sky) and seven pixels (0.35 arcsec) in cross-dispersion. The FGS effective aperture is a 5 arcsec square. For the STIS spectrophotometry to be used directly without further correction, no background sources to  $\sim 10^3$  times fainter than either calibrator can exist in the annulus of  $\sim 0.35 - 3$  arcsecs. Fortunately, imaging observations exist with other HST instruments allowing closure on this unlikely, but potentially problematic factor. P041C was observed in the WFPC2 calibration program 6934. Analysis of exposures in F450W, F555W, F606W, and F622W ruled out any neighbors in the 0.7 – 3 arcsec annulus down to 1000 times fainter than P041C. At 0.35 arcsec separation,

which would only be problematic in the original STIS cross-dispersion direction, this inspection rules out neighbors <100 times fainter than P041C, with intermediate sensitivity over the small 0.35 – 0.7 arcsec annulus. Because HD 209458 is much brighter, confounding neighbors are much less likely. Although the test is not quite as direct as for P041C, images in NICMOS F215N and ACS/HRC F330W are available from science programs 9832 and 10145, respectively. In the NICMOS image, any contaminating neighbor in the near-IR over the 2-3 arcsec annulus to  $\times 1000$  fainter can be ruled out. In the ACS/HRC image, any contaminating neighbor in the near-UV over the full 0.35-3 arcsec annulus (except for a trivial loss in bleeding columns) to  $\times 1000$  fainter can be ruled out for HD209458. For both P041C and HD 209458, there is excellent confidence that any neighbors that might be included in FGS observations, but not in the smaller aperture STIS observations, should not perturb final results for the deadtime at more than 0.1%.

A comparable error of up to 0.1% arises from noting in the full HD 17156 time series that responses during orbits show systematics with full amplitude of 0.2 – 0.3%. Averages over time scales used for the HD 209458 and P041C calibration observations brings residual offsets down to the 0.1% level.

### 3.2. FGS2r filter bandpass and PMT sensitivities

The next factor to consider is the actual FGS2r bandpass shape vs. wavelength, so that an appropriately weighted ratio can be derived from the STIS spectrophotometry.

Defining the full FGS response function to be  $fgs(\lambda)$  (product of PMT sensitivity and filter bandpass) compiled on the same 20 Å centers of the HD 209458 to P041C spectrophotometry values, we then seek the single number,  $PMT_{ratio}$  defined as:

$$PMT_{ratio} = \frac{\sum_{4200\text{\AA}}^{7200\text{\AA}} fgs(\lambda) * HD209458(\lambda)}{\sum_{4200\text{\AA}}^{7200\text{\AA}} fgs(\lambda) * P041C(\lambda)} \quad (5)$$

We have used two successive approximations to defining the  $fgs(\lambda)$  function. The first of these relies on use of the generic trace of transmission for F583W (used for all of our science and calibration observations) from Figure 2.8 of the FGS Instrument Handbook (Nelán et al. 2007) for FGS1r, and the typical PMT efficiency with wavelength plotted in Figure 2.9. These were digitized by hand from the Handbook plots, then in the case of F583W interpolated linearly to our common 20 Å grid, and in the case of PMT efficiency interpolated using a quadratic fit to graph values at 4500, 5000, 6000 and 7000 Å. This assumes the response for all 4 PMTs is identical, and that the F583W filter used in FGS2r is similar to that in FGS1r (thought to be true). Within an FGS the light passes through a single filter, so differences would arise from the photo-cathode sensitivities (likely dominant

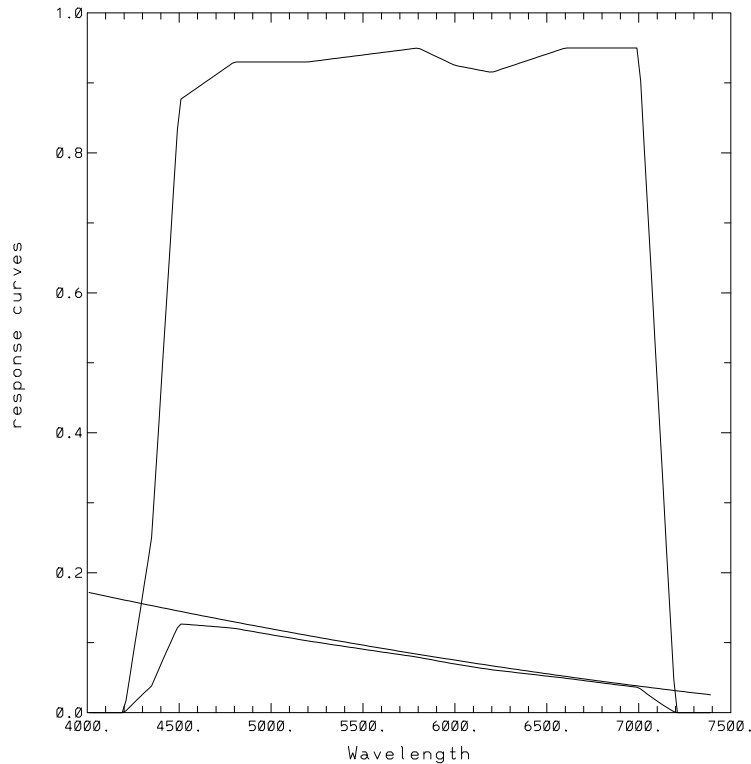


Fig. 2.— From the top the curves are: 1) F583W transmission, 2) PMT sensitivity versus wavelength, and 3) the  $f_{gs}(\lambda)$  function which is the product of the other two curves.

term of PMT-to-PMT effects), and separate reflections leading up to each PMT.

Figure 2 shows the F583W filter trace, generic PMT sensitivity, and resulting  $f_{gs}(\lambda)$  curve assumed to hold for FGS2r.

Evaluating Eq. 5 using the inputs from Figures 1 and 2 yields a  $PMT_{ratio} = 56.097$ . The pivot wavelength (effective, weighted by stellar SED, center of response) is  $5360\text{\AA}$  for HD 209458, and some  $20\text{\AA}$  redder for P041C. This is the ratio of counts for HD 209458 to P041C that the FGS2r PMTs should record after correction for background subtraction and deadtime has been made to raw 40 Hz counts. We estimated in §2 that the background correction, which is relevant only for the fainter P041C, or unaccounted for neighbors, or orbital systematics in count rate can change the calibrated count level by one part in a thousand, this implies an error on  $PMT_{ratio}$  of 0.056 (i.e., a 0.1% effect). The intrinsic error of 0.35% quoted in §3.1 translates to an error of 0.20. These are viewed as fundamental limiting factors.

Before exploring more precise representations of the FGS2r sensitivity functions it is instructive to consider what errors on  $PMT_{ratio}$  follow from assumed changes to  $f_{gs}(\lambda)$  as shown in Figure 2. Representing the generic PMT sensitivity with wavelength variation by a line, rather than a parabola results in a change a full factor of 10 below the error of 0.35%

Table 2: Laboratory measurements of FGS2r sensitivity in 1998.

Filter	$A_X$	$B_X$	$A_Y$	$B_Y$
4500	2280	2402	2988	2951
5500	2537	2951	3760	3308
6000	2344	2808	3419	2912
6500	1843	1898	2035	1760

from basic knowledge of the absolute flux ratio of our two stars. Similarly, a  $\pm 100 \text{ \AA}$  shift of the assumed red cutoff for the F583W filter results in a change of  $PMT_{ratio}$  that is still  $5\times$  smaller than the intrinsic absolute flux ratio error. A  $\pm 100 \text{ \AA}$  shift of the assumed blue cutoff for F583W has a larger impact since the PMTs have rising response in the blue; this corresponds to an error of  $\pm 0.36\%$  on  $PMT_{ratio}$  which is similar to the error resulting from the fundamental uncertainties quoted in the previous paragraph. A  $100 \text{ \AA}$  shift in blue edge cutoff is probably unreasonably large, and thanks to the relatively shallow slope in Figure 1 of the stellar count ratio (by design of choosing similar spectral types) we are only mildly sensitive to uncertain knowledge of the FGS2r response function.

Prior to flight of FGS2r extensive laboratory calibrations were performed in 1998 (Abramowicz-Reed, 2009), including a lateral color term experiment in which the relative throughput of the 4 PMTs were measured by providing a stimulus consisting of a roughly solar (5800 Kelvin) black body spectrum passed through  $100 \text{ \AA}$  filters at 4500, 5500, 6000 and  $6500 \text{ \AA}$ . This provides the basis for our second general approach to defining the  $fgs(\lambda)$  function. This has the obvious advantage of using the actual flight hardware, which includes the effects of unique mirror reflectivities and responses by PMT. It has a potential disadvantage of building in strong constraints from a measurement procedure which could itself have unknown relative errors. In the latter regard the measurement at  $4500 \text{ \AA}$  is particularly significant. This is the wavelength range at which a  $100 \text{ \AA}$  wide filter would just start to strongly sense the steep blue cutoff of F583W used in this experiment. However, differences in assumed width of the  $4500 \text{ \AA}$  filter relative to the others, or corrections for the black body illumination function could impose comparable errors. Table 2 shows these laboratory measurements.

As sanity checks on the content of Table 2, and soundness of this laboratory experiment it is informative to compare normalized partial sums over the rows and columns of Table 2. Partial sums over rows should show very similar changes row-to-row as the generic PMT sensitivity included from the FGS Instrument Handbook in Figure 2. The changes over rows do closely track the generic response, with the exception that the  $4500 \text{ \AA}$  row gives values that are nearly a factor of 2 below expectations. The latter point could be made consistent by assuming a  $70 \text{ \AA}$  shift to the red of the blue edge for F583W. Taking partials

as column sums, assuming the sum of these 4 points to be a decent reflection of a proper integral, should yield column-to-column changes similar to the actual count rates provided by the 4 PMTs. The stellar count levels show lowest to highest counts over  $A_X$ ,  $B_X$ ,  $B_Y$  to  $A_Y$  with a full range (after deadtime correction, or on a faint star like PO41C where this doesn't matter) of 1.34. The column partials from Table 2 show exactly the same order, and a full range of 1.35, with generally good correlation otherwise. This suggests generally good consistency between the laboratory measurements and recent on-orbit performance of FGS2r. It is therefore informative to adopt these values as strong constraints on the  $fgs(\lambda)$  function, this time allowing unique results for each PMT.

We turn the entries of Table 2 into new  $fgs(\lambda)$  functions as follows: (1) The responses shown in Table 2 are normalized by 5800 Kelvin black body fluxes over 100 Å intervals at the listed center wavelengths. (2) To place values on a similar scale to the generic PMT response the mean over all entries at 5500, 6000 and 6500 Å is formed, then all entries in Table 2 are normalized such that this mean is 0.1. (3) The transmission function of F583W as in Figure 2 is initially assumed to hold. (4) Steps (1)-(3) allow forming  $fgs(\lambda)$  for each PMT. Sums within these are taken in 100 Å windows at 4500 and normalized to the mean of similar 100 Å windows at 5500 and 6000 Å. (5) Adjustments of the assumed blue edge of F583W are made until the ratio returned from (4) equals (averaged over all 4 PMTs) the same ratio from the entries of Table 2 after correction for the blackbody color term. This requires a 70 Å shift to the red of the blue cutoff for F583W, this seems large, but probably not outside the realm of reasonableness. (6) Finally, sums as in step (4) are brought into agreement in detail with the same ratios from Table 2 by fudging the assumed slopes (poorly constrained, since we use the only point in the blue at 4500 Å to set the filter cutoff location) of the PMT response functions.

We make no claim that the several steps in the previous paragraph represent a unique approach to utilizing the results of the pre-flight laboratory measurements on FGS2r. However, these steps do represent a reasonable approach in which full weight is given to the purity of the laboratory measurements. Figure 3 shows the  $fgs(\lambda)$  response functions for all 4 PMTs after following the above prescription. These show overall offset in terms of total enclosed area that are similar to the actual on-orbit count levels across the 4 PMTs. With the exception of PMT  $B_Y$  all have similar general slopes, inspection of Table 2 shows that the entries are consistent with  $B_Y$  having a unique slope.

Evaluating Eq. (5) using the  $fgs(\lambda)$  of Figure 3 leads to  $PMT_{ratio} = 55.847, 55.731, 55.730, \text{ and } 55.877$  over the 4 PMTs as ordered in tables 1 and 2. The full range over the 4 PMTs is 0.15, which is slightly smaller than the overall level of uncertainty imposed by the 0.35% uncertainty of intrinsic flux ratios from STIS spectrophotometry. However, the mean value over the 4 PMTs is now 55.796 versus 56.097 derived using the generic FGS Instrument Handbook prescription, or a mean shift of 0.54% from imposing the constraints from the laboratory measurements of Table 2. Most of this change follows from the 4500

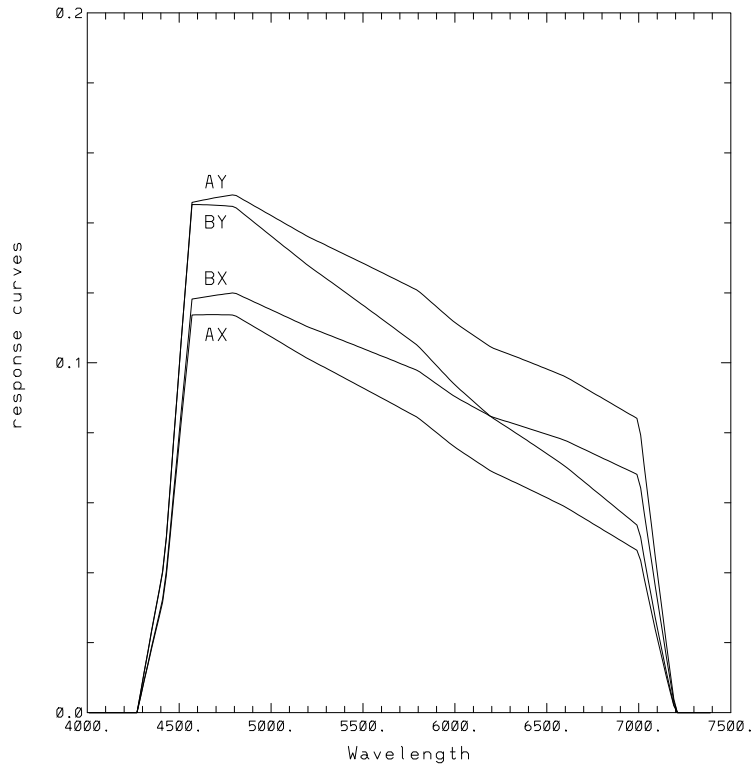


Fig. 3.— This shows the  $fgs(\lambda)$  response curves for each of the FGS2r PMTs after following the prescriptions in §3.2 to allow for pre-flight laboratory measurements.

Å relative measurements being much lower than that which would be expected from the FGS Instrument Handbook values, this has been accounted for to first order in these analyses by shifting the blue cutoff of F583W to the red by 70 Å. The mean pivot wavelength for HD 209458 in this scenario is 5500Å , changes across PMTs reach 70Å , but the PMT pairs both closely average to  $\sim 5500\text{Å}$  as effective central wavelengths.

### 3.3. Derivation of deadtime correction for each PMT

With the target  $PMT_{ratio}$  derived under two assumptions in §3.2 we are now ready to use these in a derivation of deadtime correction coefficients for each PMT. Since the counts for both P041C and HD 209458 will be altered by application of the deadtime correction, we must either iteratively solve for a deadtime that yields the desired ratio, or apply a grid-search technique that effectively does the same thing. We adopt the latter for simplicity. The procedure now is to read in all of the 40 Hz samples for both P041C and HD 209458, then over a grid of assumed deadtimes (200 - 320 nano-seconds suffices) correct each data value of each PMT at the 40 Hz level (apply Eq. 3). Then means for each star by each PMT are taken and the ratio of counts measured by FGS2r printed out over deadtimes of 190, 191 . . . 320 nano seconds. Then on a PMT-by-PMT basis linear interpolation to the target

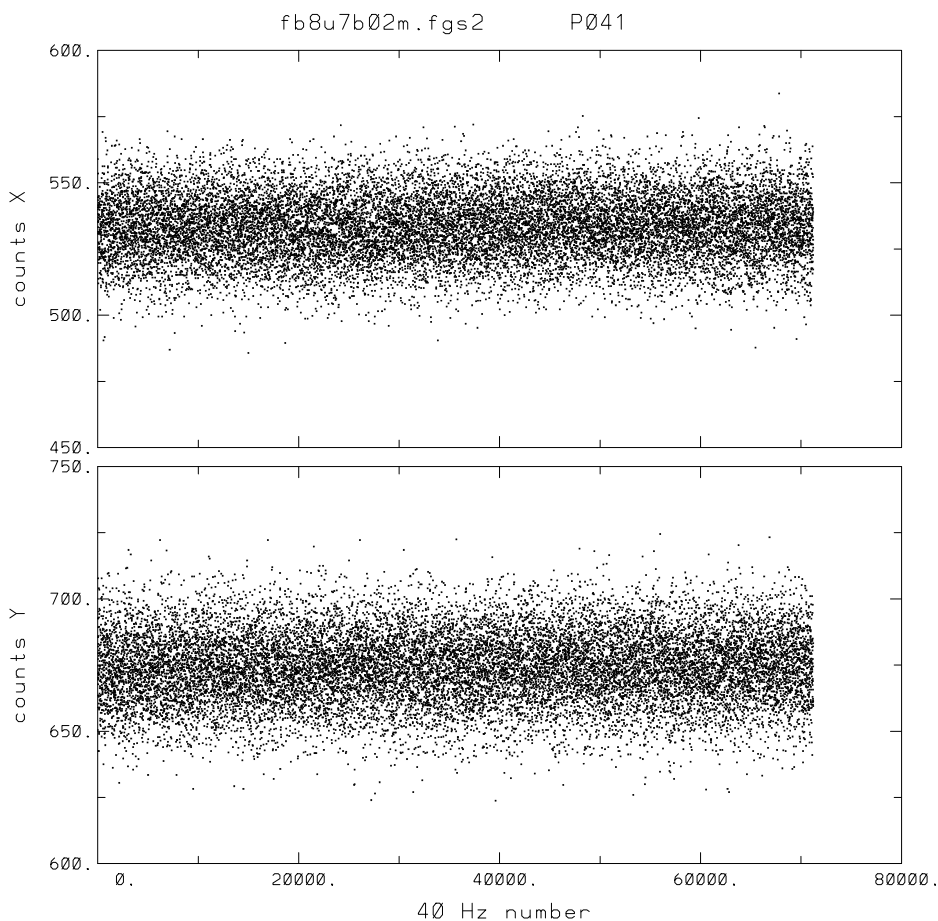


Fig. 4.— Time series for the single orbit of P041C data in POS mode with FGS2r. Counts have been summed by PMT  $X$  and  $Y$  pairs. No deviations are seen, showing that the full set of P041C data may be averaged to arrive at a mean for each PMT. For control of file size averages over four successive points are plotted here.

deadtime is performed.

Before performing the last step we carefully inspect time series of P041C and HD 209458, as was done for the dark data in §2, in order to check for any anomalies in the time series. The P041C data appeared benign, the counts over time reflected a constant level with random fluctuations as expected. Figure 4 shows the time series of the PMTs for P041C observations after summing the PMTs by pairs. This rules out one potential source of error in our experiment, had the P041C observations been taken at a time of unusually high sky, or had these been taken during an orbit that grazed the SAA, variations in time would have been evident. For the factor of 55 brighter HD 209458 it is essentially impossible for sky (or brief SAA induced particle counts) to matter for a sum formed over some 40 minutes. However, the HD 209458 time series did exhibit a different type of problem.

Figure 5 shows the time series for HD 209458, again after summing into the  $X$  and  $Y$

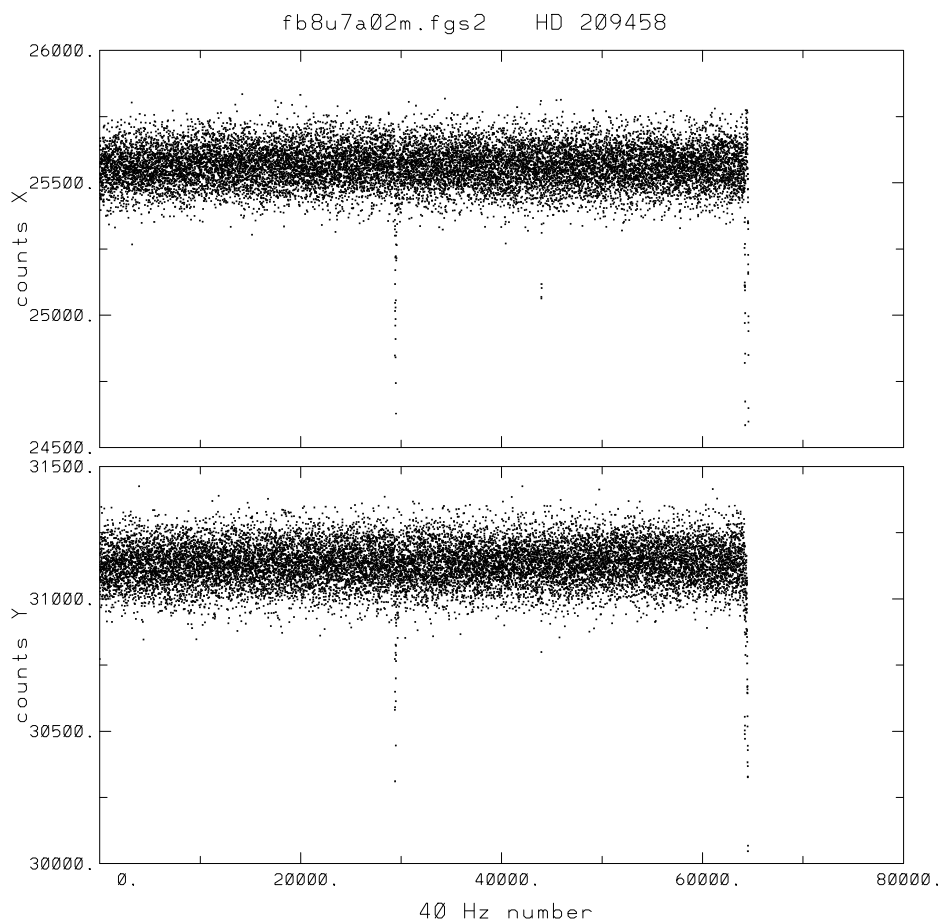


Fig. 5.— Times series for the single orbit of HD 209458 data with FGS2r in POS mode. Counts have been summed by PMT  $X$  and  $Y$  pairs. Loss of lock is indicated by a rapid drop near the end. As discussed in the text periods of low counts have been excised before forming sums. To control file size averages over four successive points have been plotted.

PMT pairs. At the end of the plotted series the counts rapidly transition to near zero, lock on HD 209458 was evidently lost near 40-Hz number 64000. The counts after this remain near zero until the time series end some 7700 40-Hz steps later. For the purposes of forming a mean count level the time series was truncated before the precipitous drop, and a small region near 40-Hz number 29000 when the counts drop noticeably low in both  $X$  and  $Y$  PMT pairs was also excised from statistics. The final time series uses a total of 63,644 40-Hz samples, or 26.5 minutes. We note that in some 175 orbits on HD 17156 in GO/DD-11945 a similar loss of lock and transition to near zero counts happened only one time. This raises a caution that with the even brighter HD 209458 the chances of losing lock may be increased. Similarly in the 150 orbits of data on HD 17156 in the intensive 10-day time series there was never an excursion analogous to the drop near 40-Hz step number 29000 as seen in Figure 5. Having excised the suspect data points these observations appear robust for determining mean counts on each PMT individually for both P041C and HD 209458.

Table 3: Deadtime corrections in nano-seconds based on P041C and HD 209458 observations.

Case	$A_X$	$B_X$	$A_Y$	$B_Y$
Eq. (3) – Nonparalyzable				
1	218.5	317.0	268.9	291.4
2	210.6	306.0	260.3	286.0
Eq. (4) – Paralyzable				
1	205.5	289.4	244.0	263.8
2	198.5	280.3	236.9	259.3

Table 3 presents the deadtimes in units of nano-seconds for the two treatments of FGS sensitivity with wavelength discussed in §3.2, and for the Nonparalyzable and Paralyzable detector options of Eqs (3) and (4) respectively. Case 1 assumes the F583W filter transmission and generic PMT response curve from the FGS Instrument Handbook (Nelán et al. 2007). Case 2 assumes modifications to both the F583W filter transmission and response functions for the individual PMTs as a function of wavelength to match the laboratory measurements of sensitivity conducted pre-launch of FGS2r as shown in Table 2. The  $PMT_{ratio}$  for the generic Case 1 is 56.097, for Case 2 the target  $PMT_{ratio} = 55.847, 55.731, 55.730, \text{ and } 55.877$ .

The Case 2 deadtimes in which pre-launch laboratory measures were enforced for the PMT sensitivity function range from 1.7 to 3.7% smaller than those that would be derived from simply adopting the canonical Handbook constraints.

### 3.4. Non-linear HSP deadtime and retirement as concern for FGS2r

The High Speed Photometer (HSP; Bless et al 1992) was a first generation instrument on HST that included (among other detectors) a PMT. While neither the detectors, nor presumably the electronics are closely similar across the HSP and FGS, an examination of deadtime calibration for the HSP raises a note of caution. Both systems are photon counting devices suffering from deadtime effects. In the case of HSP the inherent deadtime is significantly smaller at 42 nano-seconds relative to the 200-300 ns of FGS. Usually the HSP was operated in a pulse-counting (“digital”) mode, but it also had the capability of reading out the current from the detector (“analog” mode). The current measurement was noisier than the digital count rate but had the advantage that it was not subject to dead time effects, so it gave linear measurements for much brighter sources. It was also possible to collect both digital and analog measurements simultaneously, which was useful for calibration.

On 1990 November 8 the HSP PMT was used in the combined digital/ analog readout mode to observe the bright earth (dataset v0e10109t). The sample time for the data was

5 milliseconds, with a total integration time of 5 minutes (59,904 samples). During the observations the earth, as seen through the 1 arcsec diameter PMT aperture, varied by more than a factor of 4, occasionally saturating the 12-bit A/D converter for the current measurement; consecutive 5 ms samples varied by as much as a factor of 2.5. The analog saturation level corresponds to a count rate of  $7.6 \times 10^7$  cts/ s. About 165 seconds into the observation, the PMT aperture passed off the edge of the bright earth and the count rate gradually declined to about  $1 \times 10^5$  cts/s.

This wide range of count rates with simultaneous analog and digital measurements is ideal for exploring the dead time behavior of the HSP PMT pulse-counting electronics at very high count rates. The top panel of Figure 6 shows the digital count rate versus the analog count rate (converted to an equivalent digital rate) for each of the 5 msec samples. The blue line is the usual dead time model where the observed count rate  $S$  is related to the true count rate  $R$  by  $S = R/(1 + Rt)$ , where  $t = 40$  ns is the dead time. For high count rates this model is clearly inadequate, and in fact the observed count rate does not even increase monotonically with the true rate. The likely explanation for this behavior is that the pulses from different counts overlap to produce a (roughly) steady current out of the detector, leading the pulse-height discriminator (effectively a high- pass filter) to fail to detect a pulse that exceeds the detection threshold for many of the counts. As the count rate increases further, eventually the current fluctuations from groups of counts become large enough to trigger the pulse-height discriminator and the observed count rate starts to rise again.

The red line is an empirical fit using the usual dead-time equation given above but with an effective dead time  $t_{eff}$  that is a quadratic function of the count rate instead of a constant. The bottom panel shows the effective dead time for each data point. Note the scatter is large for low count rates because the dead time correction itself is small, so the uncertainties in  $t_{eff}$  are large. For nominal dead time corrections  $Rt = 0.1, 0.15, 0.2,$  and  $0.25$ , the observed count rate falls below the simple model prediction by 0.6%, 2.0%, 4.5%, and 8.1% respectively.

Since the correction for deadtime in our HD 209458 observations peaks at 21% for the  $B_Y$  PMT, a similar issue with the FGS response could lead to an error of 5% in the implied, corrected counts. While there is no reason to expect the independent detector technology and electronics of the FGS should closely repeat the HSP behavior, the existence of this effect in the HSP seriously erodes confidence that equations as simple as Eqs. (3) and (4) hold over the regime up to 21% corrections as needed for our calibrations.

An ideal calibration for FGS deadtime would need to utilize additional stars, with closely similar spectral types that have brightness intermediate to our P041C and HD 209458 calibrators. We do have excellent measures of count rates for our science target at  $V = 8.17$ , and for the  $V = 9.56$  FGS calibration standard Upgren 69. Without available absolute spectrophotometry on a common system as from the STIS observations of P041C and HD 209458 we cannot use these additional targets as true calibration points. However, they will

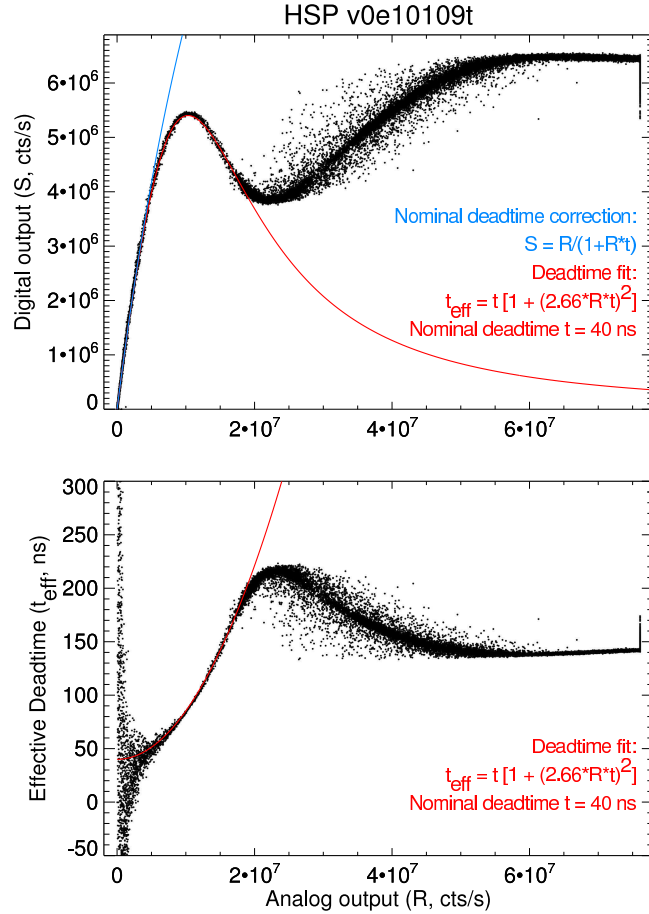


Fig. 6.— HSP digitized counts versus current-mode measurements (White 2009). The upper panel shows a standard fit to the data using a nominal deadtime correction that works adequately for very small adjustments (left – blue, monotonic curve), an empirical fit is shown (right curve – red) allowing a flux dependent change in the deadtime itself that fits the data much better. Only data up to about analog of  $7 \times 10^6$ , and digital to  $5 \times 10^6$  are relevant for consideration with respect to FGS. The lower panel shows the effective deadtime versus input signal level. The initial rise to maximum, then decline in digital counts is characteristic of a Paralyzable system, while the eventual rise to constant output is characteristic of a Nonparalyzable system.

suffice as sanity checks sufficient to rule out deviations from the simple level of Eqs. (3) and (4) at levels well below effects noted on HSP. We will approach this from two directions: (1) Simply noting the count levels corrected for deadtime for each star for each PMT, and seeing if these scale with  $V$  magnitude (which fortunately is a close match to the FGS bandpass). (2) Taking advantage of the fact that the intrinsic sensitivity and associated deadtime constants across the 4 PMTs lead to largely variable corrections – from 0.12 to 0.21 for HD 209458. If a simple deadtime correction (i.e. there is a single constant  $T_D$  per PMT as in Eqs. (3) or (4)) holds, then corrected ratios of stars counts across the PMTs should be

Table 4: Original and deadtime corrected counts by star and PMT.

Star	$V, B - V$	$A_X$	$B_X$	$A_Y$	$B_Y$	$A_X$	$B_X$	$A_Y$	$B_Y$	$Y/X$	Ratio
Counts without deadtime correction.											
—— Direct counts ——      – Normalized counts –											
P041C	12.005,0.61	256.79	269.95	342.80	326.68	.859	.903	1.146	1.092	1.2710	0.857
Upgren69	9.56,0.48	2429.2	2427.4	3160.3	2979.2	.883	.883	1.149	1.084	1.2642	0.886
HD 17156	8.17,0.59	8294.7	8320.7	10589.	9947.7	.893	.895	1.140	1.071	1.2360	0.943
HD 209458	7.65,0.59	12819.	12739.	15982.	15146.	.905	.899	1.128	1.069	1.2179	—
Counts with deadtime correction: Eq. (3) – Nonparalyzable											
P041C	12.005,0.61	257.37	270.87	344.05	327.92	.858	.903	1.147	1.093	1.2721	1.011
Upgren69	9.56,0.48	2479.5	2502.2	3268.4	3083.8	.875	.883	1.153	1.088	1.2751	1.017
HD 17156	8.17,0.59	8919.3	9266.2	11903.	11226.	.866	.895	1.153	1.087	1.2718	1.004
HD 209458	7.65,0.59	14373.	15096.	19175.	18323.	.859	.902	1.145	1.094	1.2725	—
Counts with deadtime correction: Eq. (4) – Paralyzable											
P041C	12.005,0.61	257.34	270.79	343.94	327.81	.859	.903	1.146	1.092	1.2719	1.011
Upgren69	9.56,0.48	2477.0	2496.8	3259.9	3075.2	.876	.883	1.153	1.088	1.2737	1.019
HD 17156	8.17,0.59	8903.7	9229.8	11849.	11171.	.865	.897	1.152	1.086	1.2695	1.008
HD 209458	7.65,0.59	14371.	15091.	19168.	18318.	.859	.902	1.145	1.094	1.2723	—

Photometry references – P041C: Casagrande et al 2006, Upgren 69: Stetson et al 2004, HD 17156: ESA 1997, HD 209458: Butler et al 2006.

independent of stellar magnitude. If a simple correction, as with HSP, does not hold these ratios should show changes with magnitude, even though by design they are set to common values for our two primary calibration stars.

Table 4 reviews published photometry for the four stars observed for these calibrations, mean counts in each PMT before deadtime correction (but with background subtraction), and mean counts in each PMT after deadtime correction using Case 2 of Table 3. The columns labeled ‘Normalized counts’ are simply the ‘Direct counts’ across the 4 PMTs normalized to the mean over all 4 PMTs. The column  $Y/X$  shows the ratio after summing over the  $A$  and  $B$  PMTs of each side, note that the mean count levels for the  $Y$  side are some 27% higher than for the  $X$  side PMTs. The final column marked ‘Ratio’ is the ratio of counts for HD 209458, averaged over all 4 PMTs, to the counts for each star divided by the predicted ratio based simply on the  $\delta V$  magnitude. By definition the entry for HD 209458 is thus unity. By design the P041C entry after deadtime correction for the ‘Ratio’ column is unity for the assumed ratio of counts provided by the STIS spectrophotometry; the difference of  $V$  magnitudes closely, but not identically matches the STIS spectrophotometry in this case. Before deadtime correction the entries in Table 4 for  $Y/X$  and ‘Ratio’ show large deviations

over the 4 stars in the sense expected of having a significant deadtime effect on the brighter stars. After deadtime correction these entries for P041C and HD 209458 are expected to be essentially identical by design, since the relative counts in these stars provided the deadtime coefficients. The effective deadtime corrections for each star, e.g. based on Eq. (3) can be found by ratioing the direct counts after correction to those before, e.g. for HD 209458 these are 1.121, 1.185, 1.200, and 1.210; for HD 17156 these are 1.075, 1.114, 1.124, and 1.128. The mean correction for deadtime is 35% larger for the  $Y$  relative to  $X$  PMTs. Were the deadtime corrections for FGS to show a nonlinearity at the level seen by HSP, then between the HD 209458 and HD 17156 entries for  $Y/X$  we would expect to see a difference of about 2%, but instead see constancy to a factor of  $\gtrsim 30$  better than this. The ‘Normalized counts’ entries for HD 17156 are derived as a mean over 101 independent visits. Over this large number of independent trials each PMT individually shows a scatter of 0.0022, while the corresponding  $Y/X$  value is much more stable at a scatter of 0.0007. Similarly, an HSP-like effect would be expected to yield corrections as seen in the ‘Ratio’ column off by a couple of per cent, while the result is as good (if not better) as can be expected given the quality of supporting relative photometry. We can effectively rule out a non-linearity in deadtimes as seen with HSP over the correction levels relevant to FGS2r. The highly consistent results seen in Table 4 suggest that no additional error budget needs to be included for a potential non-linearity factor.

Another factor that the small scatter in Table 4 effectively eliminates are potential problems with linearly polarized sources contaminating these calibrations. The FGSs function by using a linear-polarization based beamsplitter to initially divide the counts into the  $X$  and  $Y$  channels. If any of the stars in Table 4 had significant polarization this could shift counts between  $X$  and  $Y$  PMT pairs. Seeing nearly identical  $Y/X$  ratios for each star we posit that polarization of these sources is not an important issue.

### 3.5. Estimated errors on deadtime corrections

We presented estimates of errors on the known flux ratio of HD 209458 to P041C which determine these deadtime calibrations, of  $<0.1\%$  arising from uncertainty in backgrounds affecting the P041C counts, and  $0.35\%$  as a  $1\text{-}\sigma$  estimate of the uncertainty from supporting STIS spectrophotometry. Both of the above errors are considered random. A source of systematic uncertainty arises through the spectrophotometric ratio of these two stars not being a constant, coupled with the uncertainties in FGS response with wavelength discussed in §3.2. We do not have a robust estimate of what error to adopt for the uncertain FGS response function, but settle on assuming an additional range of  $-0.15\%$  on the  $PMT_{ratio}$  values for Case 2 of §3.3, to  $+0.55\%$  (which takes the values back to Case 1). Extending the  $-0.15\%$  to  $0.55\%$  systematic range with the random  $0.35\%$  sets the full range of input flux ratio uncertainty at  $-0.5\%$  to  $+0.9\%$ .

Table 5: Range of deadtime corrections from error budget in nano-seconds.

Case	$A_X$	$B_X$	$A_Y$	$B_Y$
-0.5%	201.7	297.5	253.5	279.0
Case 2	210.6	306.0	260.3	286.0
+0.9%	226.4	321.0	272.1	298.4

Table 5 shows the resulting estimates for deadtime corrections assuming the -0.5% to +0.9% changes in  $PMT_{ratio}$ , using Eq. 3 for the Nonparalyzable assumption and repeats the central value corresponding to Case 2 of Table 3.

When projected to effects for the HD 17156 count levels after deadtime correction, the -0.5 to +0.9% errors assumed on the flux ratio inputs translate to -0.32% to +0.56% changes on the corrected count levels. There is no dependence of this relative error on PMT. For a nominal transit depth of 0.5% this relative error range corresponds to changes in transit depth of -16 to +28 ppm. As argued in the introduction, the formal photon statistics limited error on transit depth determinations is  $\sim 20$  ppm per transit. Systematics associated with photometric changes correlating with the HST orbital period are likely to limit determinations to well above this formal Poisson value. Therefore the deadtime has been calibrated sufficiently well that residual errors on its application, while not completely insignificant, are only modest factors in interpretations involving estimates of the relative transit depth in this case with order 10,000 counts per 40-Hz sample per PMT.

The above discussion in §3.5 was under the assumption of Eq. (3) for a Nonparalyzable detector. The deadtime corrected counts in Table 4 average 0.39% lower if Eq. (4) and Paralyzable are assumed. While from general principles we think it more likely the FGS system is Nonparalyzable, the simple solution here is to adopt Eq. (3), and extend the error estimates of -0.32% to +0.56% in estimating the true count level to absorb the systematic of -0.39% that would follow if Eq. (4) should be used. This results in -0.7% to +0.6% in corrected count levels, or up to 35 ppm errors on hypothetical 0.5% deep transits.

The  $Y/X$  entries before and after deadtime correction in Table 4 can be used to provide a sensitive consistency check on the relative deadtime corrections of the two PMT pairs. The  $Y/X$  value without deadtime correction shows a progressive change over the 4 stars, while after correction it is nearly constant. Regressing  $Y/X$  against the mean correction resulting from applying deadtime results in a linear correlation coefficient of 0.998, and an asymptotic value of 1.2716 projected for count levels low enough that no deadtime correction is needed. The mean difference of  $Y/X$ , after application of the standard (Case 2 of Table 3 for Eq. 3) deadtime correction, from this asymptotic value is 0.0013. By contrast, if we were to recompute counts assuming the deadtimes are set to the -0.32% values for  $X$  PMTs,

Table 6: Sensitivity coefficients,  $C_r$ , by PMT for FGS2r.

$A_X$	$B_X$	$A_Y$	$B_Y$
1650.2	1733.3	2201.1	2109.9

and +0.56% values for  $Y$  PMTs of Table 5, then from faint to bright stars the  $Y/X$  ratio after deadtime corrections are 1.272, 1.278, 1.283 and 1.291 respectively. Since these latter values show an order of magnitude greater deviation from the asymptotic value, than those after standard deadtime corrections, we may conclude that the relative deadtime coefficients across the  $X$  and  $Y$  pairs are known to an order of magnitude better than implied by the full allowed error range.

## 4. Sensitivity

For completeness we derive the sensitivity in units of deadtime corrected counts in 40-Hz samples for each FGS2r PMT. Assuming the equation:

$$C_T = C_r * 10.0^{0.4*(10.0-V)} \quad (6)$$

the coefficient  $C_r$  is shown in Table 6.

Also for completeness, the saturation of the FGS2r digital counting register occurs when the observed, uncorrected counts reach  $2^{16} = 65536$ , i.e. at  $V = 7.465$  for FGS2r. Errors on the deadtime corrections of Table 5 lead to errors on this limiting magnitude of 0.01. To allow a buffer of  $3\sigma$  on the assumed deadtime correction, and  $5\sigma$  fluctuations in the Poisson realizations would require keeping  $V > 7.53$ , plus an allowance for appropriate errors on the magnitude itself, and consideration of color terms if the star is not roughly solar.

## 5. Photon Aging

Since there was an identified, albeit remote, engineering concern that exposure of the PMTs to a summed flux of order  $10^{12}$  could lead to a significant loss of sensitivity we report two independent determinations of this here. The  $V = 9.56$  FGS standard calibration star Upgren 69 was observed in visits 80 and 81 shortly before and after the 10-day run on HD 17156 specifically to allow tracking this effect. Long term changes in the HD 17156 flux over the 10 days also provide a measure of this effect. Table 7 presents the inferred change of sensitivity across the 10 days using these two approaches.

Table 7: Sensitivity loss in % across 10 days observing HD 17156 with FGS2r.

Star	$A_X$	$B_X$	$A_Y$	$B_Y$	Mean
Upgren 69	-0.77	+0.23	+0.21	-0.66	-0.24
HD 17156	-0.61	-0.35	-0.39	-0.59	-0.48

The large changes seen within PMT pairs for Upgren 69 are consistent with visit-to-visit changes in the balance between the  $A$  and  $B$  PMTs of a pair due to the difference in where FGS2r locked onto the S-curves. Each finelock acquisition seeks out the value of the S-curve that corresponds to  $(A_{ave} - B_{ave})/(A_{ave} + B_{ave})$ , where  $A_{ave}$  and  $B_{ave}$  are the average of sixteen 40-Hz samples that were gathered at the very start of the walkdown to finelock. Since PMT shot noise affects this balance, we can expect the FGS to seek out slightly different places on the S-curve each visit. The entries for HD 17156 follow from fitting a line to 101 independent measures over 9.67 days, and evaluating the slope times 9.67 days divided by the mean. The HD 17156 entries should be nearly free of influences following from the visit-to-visit balance changes (the effect visit-to-visit is inherently smaller to start with for this brighter star). It is safe to conclude that observations resulting in exposure to a total of  $10^{12}$  photons summed over all four PMTs resulted in less than a 1% degradation in any of the PMTs, and that the mean degradation is  $0.4 \pm 0.2\%$ . This implies as a practical matter that observations of this type do not pose a concern in terms of FGS lifetime.

## 6. Noise Properties of Deadtime Corrected FGS Data.

Not only will deadtime effects in photon counting devices reduce the true count rate to a lower measured rate, these effects will also change the statistical distribution.

We have in hand corrections that take detected counts per 40-Hz sample into estimates for the true count rate. Desired here are estimates for what the variance should be in either of these spaces.

Evans (1955) provides estimates for the variance in regimes appropriate to both our Eq (3) – Nonparalyzable, and Eq. (4) – Paralyzable.

For the Nonparalyzable case, following from Eq. (3) the variance in the measured count space:

$$\sigma^2 \approx C_T / (1.0 + C_T(T_D/T_I))^3 \quad (7)$$

For the Paralyzable case, following from Eq. (4) the variance in the measured count

space:

$$\sigma^2 = C_T(1.0 - 2 * C_T(T_D/T_I) + C_T(T_D/T_I)^2) \quad (8)$$

Zhang et al (1995) present the same Eq. (8), but had typos that incorrectly show measured, rather than the proper true counts.

It is instructive to consider specific cases. Consider the implied scatter for a time series in which the expectation value for  $C_M = 10000$ . and the corresponding  $C_T = 11183.25$  (as would hold for  $D_T = 250$  ns and Eq. 4). Here the inferred scatter on  $C_M$  is 90.2 for a  $S/N = 110.86$ .

A similar estimate for the Eq. (3), Nonparalyzable case returns a  $S/N = 107.32$ .

The true count level of 11183.25 in this sanity check would translate to a Poisson limited  $S/N = 105.75$ . Thus, the estimated  $S/N$  under either scenario is better than the Poisson limit on the true count rate. It is clear why this can happen by considering the nonparalyzable case at very high input levels, in this regime the count rate saturates at  $1/T_D$ , and a time series consisting of measured counts in this case would have zero variance. In this extreme example any true variations in the input signal are completely destroyed.

Rather than adopting estimates from Eqs (7) or (8) that yield  $S/N$  above the Poisson limit on the input counts, we will simply adopt the Poisson limit on the input counts as the best noise estimate available.

## 7. Summary.

Observations of two calibration stars, P041C and HD 209458, with excellent STIS spectrophotometry have been used to establish accurate calibrations of deadtime corrections for each FGS2r PMT as needed in support of a recent large science program. Uncertainties on the deadtime calibration are sufficiently small as to comprise only a modest contribution to the error term in analyzing the science data.

Calibrations were also obtained that establish the background count level for the FGS2r PMTs, the sensitivity of each PMT, and the expected level of PMT sensitivity loss with exposure to large photon fluxes.

We thank Linda Abramowicz-Reed for communications on laboratory testing of FGS2r pre-flight. Rick White provided the figures and discussion related to the deadtime behavior of HSP, and generally useful discussion. We thank Merle Reinhart in particular for expertly drafting and guiding the observations in GO/DD-11945 and Mike Wenz at Goddard for shepherding the proposal through pre-flight reviews and monitoring engineering performance

during execution. We thank the STScI Director, Matt Mountain, for the DD time award that motivated these calibrations.

## References

- Abramowicz-Reed, L. 2009, personal communication.
- Bless, R.C., Percival, J.W., Walter, L.E., & While, R.L. 1992, “High Speed Photometer Instrument Handbook”, Version 3.0, (Baltimore: STScI)
- Bohlin, R. C. 2007, in ASP Conf. Ser. 364, The Future of Photometric, Spectrophotometric, and Polarimetric Standardization, ed. C. Sterken (Ann Arbor, MI: Sheridan Books), p. 315; also arXiv:0608.715
- Bohlin, R. C., Dickinson, M. E., & Calzetti, D. 2001, AJ, 122, 2118
- Bohlin, R. C., & Gilliland, R. L. 2004, AJ, 128, 3053
- Bohlin, R. C., Riess, A., & de Jong, R., 2006, Instrument Science Report, NICMOS 2006-002, (Baltimore: STScI)
- Butler, R.P. et al. 2006, ApJ, 646, 505
- Casagrande, L. Partinari, L., & Flynn, C. 2006, MNRAS, 373, 13
- ESA. 1997, The Hipparcos and Tycho Catalogues, (ESA SP-1200; Noordwijk: ESA)
- Evans, R.D. 1955, Atomic Nucleus (New York: McGraw-Hill)
- Goudfrooij, P., & Bohlin, R. C. 2006, Instrument Science Report, STIS 2006-03, (Baltimore: STScI)
- Lattanzi, M.G., & Taff, L.G. 1993, “FGS Instrument Report No. 23”.
- Nelan, R., et al. 2007, “Fine Guidance Sensor Instrument Handbook”, Version 16.0, (Baltimore: STScI)
- Stetson, P.B., McClure, R.D., & VandenBerg, D.A. 2004, PASP, 116, 1012
- Stys, D. J., Bohlin, R. C. & Goudfrooij, P. 2004, Instrument Science Report, STIS 2004-04, (Baltimore: STScI)
- White, R.L. 2009, personal communication.
- Zhang, et al. 1995, ApJ, 449, 930.